Characterization of the NTPase, RNA-Binding, and RNA Helicase Activities of the DEAH-Box Splicing Factor Prp22†

Naoko Tanaka and Beate Schwer*

Department of Microbiology and Immunology, Weill Medical College of Cornell University, 1300 York Avenue, New York, New York 10021

Received March 3, 2005; Revised Manuscript Received May 12, 2005

ABSTRACT: The DEAH protein Prp22 is important for the second transesterification step of pre-mRNA splicing, and it is essential for releasing mature mRNA from the spliceosome. Recombinant Prp22 has RNA-stimulated ATPase and ATP-dependent unwinding activities, which are crucial for the mRNA release step. In this study, we characterize the RNA-binding, NTP hydrolysis, and RNA unwinding functions of Prp22. Using nitrocellulose filter binding assays, we determined that the apparent affinity of Prp22 is ∼20-fold greater for single-stranded RNA than for single-stranded DNA or duplex nucleic acids. Inclusion of hydrolyzable ATP in binding reactions increased the apparent K_D for RNA by 3−4-fold. The Prp22−RNA interaction is influenced by the length of the RNA chain, and the apparent K_D values for poly(A)$_{40}$ and poly(A)$_{10}$ are 17 and 140 nM, respectively. RNA-stimulated ATP hydrolysis is similarly affected by chain length, and optimal activity requires RNA oligomers of ≥20 nt. We show that Prp22 can hydrolyze all common NTPs and dNTPs with comparable efficiencies and that Prp22 unwinds RNA duplexes with 3′ to 5′ directionality.

The spliceosome, a large and dynamic ribonucleoprotein complex, catalyzes intron excision from pre-mRNAs.[1] Conformational rearrangements of RNA−RNA, RNA−protein, and protein−protein interactions are crucial for accurate splice site recognition, for bringing the splice sites into proximity for catalysis, and for product release during spliceosome disassembly (*1*, *2*). ATPases of the DExD/H-box family provide a major driving force for structural changes in the spliceosome (*3*). DExD/H-box proteins are defined by seven motifs important for ATP binding and hydrolysis (*4*−*6*). Whereas ATPase activity appears to be a common biochemical feature of all DExD/H-box proteins tested, helicase activity, which is typically measured as the ability to unwind RNA duplexes, has been more elusive. Because DExD/H proteins participate in RNA transactions within the spliceosome, and because the relevant RNA helices may not be very extensive, it had been proposed that the biochemical repertoire of DExD/H proteins includes remodeling of RNA−protein interactions (*7*−*9*). Active displacement of a protein from single-stranded RNA has been demonstrated for the prototypical DExH-box helicase NPH-II, providing proof of principle for an RNPase activity (*10*, *11*). Genetic data showing that the requirement for the DEAD-box proteins Sub2 and Prp28 could be bypassed in vivo by deletion of the nonessential RNA-binding protein Mud2 or by specific mutations in the essential U1-C protein, respectively, lent further support to the hypothesis that disruption of RNA−protein contacts is a biologically relevant activity of RNA helicases (*12*, *13*).

Prp22 is an exemplary DEAH-box protein that functions at two distinct steps during the splicing cycle; the protein is important for the second transesterification reaction, and it catalyzes the release of mature RNA from the spliceosome (*14*−*16*). Purified Prp22 exhibits ATPase activity that is stimulated by RNA (*15*, *16*). Using double-stranded RNAs with single-stranded tails, it was shown that Prp22 is capable of unwinding helices in an ATP-dependent fashion (*15*, *16*). The ATPase activity is essential for the function of Prp22 to release mRNA from the spliceosome, insofar as ATPase-defective Prp22 mutants are invariably lethal and fail to catalyze mRNA release in vitro (*17*−*19*). Although necessary, ATPase activity is not sufficient for biological function, because mutations of Prp22 that uncouple ATPase and helicase activities are deleterious (*17*, *19*, *20*). On the basis of these findings and on genetic suppression data, it has been proposed that Prp22 uses the energy of ATP hydrolysis to disrupt interactions between the spliced mRNA and components in the spliceosome, in particular, the U5 snRNP (*19*).

Here we address several outstanding questions regarding the enzymatic activities of Prp22, including nucleotide specificity and directionality. Prp22 hydrolyzes all common NTPs and dNTPs with similar K_m and k_{cat} values. We find that Prp22 unwinds duplex nucleic acids with a single-stranded 3′-tail but not duplexes with a 5′ single-stranded tail. The 3′-tail must be RNA, whereas the displaced strand can be either RNA or DNA. These findings classify Prp22

† This work was supported by NIH Grant GM50288.

* Corresponding author. E-mail: bschwer@med.cornell.edu. Phone: 212-746-6518. Fax: 212-746-8587.

[1] Abbreviations: Prp, precursor RNA processing; pre-mRNA, precursor messenger RNA; Tris, tris(hydroxylmethyl)aminomethane; DTT, dithiothreitol; EDTA, (ethylenedinitrilo)tetraacetic acid; SDS, sodium dodecyl sulfate; PAGE, polyacrylamide gel electrophoresis; BSA, bovine serum albumin; NTP, nucleoside triphosphate; AMP-PCP, β,γ-methyleneadenosine 5′-triphosphate; bp, base pair(s); nt, nucleotide(s).

10.1021/bi050407m CCC: $30.25
Published on Web 06/18/2005

as a unidirectional 3′ to 5′ helicase. Unwinding activity and relative duplex stability showed an inverse relationship, suggesting that Prp22 per se is unlikely to be a processive helicase.

MATERIALS AND METHODS

Expression and Purification of Recombinant Prp22. pET16b-prp22 (*15*) was transformed into *Escherichia coli* strain BL21-Codon Plus(DE3)RIL (Stratagene). A culture was inoculated from a single colony of freshly transformed cells and maintained in exponential growth at 37 °C in LB medium containing 0.1 mg/mL ampicillin to a final volume of 10 L. When A_{600} reached 0.6−0.8, the culture was chilled on ice for 30 min, and production of recombinant His_{10}-Prp22 was induced by adding isopropyl β-D-thiogalactopyranoside (IPTG) to 0.4 mM and ethanol to 2% (v/v). The culture was incubated for 16 h at 17 °C with constant shaking. Cells were harvested by centrifugation and stored at −80 °C.

All subsequent operations were performed at 4 °C. The cell pellets were suspended in 500 mL of buffer A (50 mM Tris-HCl, pH 7.4, 250 mM NaCl, 10% sucrose), and lysozyme was added to 0.2 mg/mL. The suspension was mixed gently for 30 min and then adjusted to 0.1% Triton X-100. The lysate was sonicated to reduce viscosity, and insoluble material was removed by centrifugation for 30 min at 14000 rpm in a Sorvall SS34 rotor. Protease inhibitor (Complete; Roche Applied Science) was added to the soluble lysate, and the lysate was stirred for 1 h and then filtered (0.45 μm). Aliquots of 100−200 mL were loaded onto 5 mL nickel-charged HiTrap chelating columns (Amersham) equilibrated in buffer E (50 mM Tris-HCl, pH 7.4, 250 mM NaCl, 10% glycerol). The columns were washed with 25 mL of buffer E followed by 50 mL of buffer E containing 25 mM imidazole (buffer E_{25}) and 50 mL of buffer E containing 100 mM imidazole (buffer E_{100}). Bound His_{10}-Prp22 was eluted with a 50 mL gradient of 100−500 mM imidazole in buffer E. The polypeptide compositions of the fractions were monitored by SDS−PAGE analysis and staining with Bio-Safe Coomassie dye (Bio-Rad). Peak fractions containing His_{10}-Prp22 were pooled, and ammonium sulfate was added to achieve 40% saturation. The protein precipitate was collected by centrifugation for 30 min at 14000 rpm in a Sorvall SS34 rotor and resuspended in 10 mL of buffer D (50 mM Tris-HCl, pH 7.4, 2 mM DTT, 1 mM EDTA, 10% glycerol) containing 150 mM NaCl. The protein solution was filtered (0.22 μm), and a 5 mL aliquot was applied to a 320 mL HiLoad Superdex 200 prep grade column (Amersham), equilibrated with buffer D containing 150 mM NaCl, and eluted with the same buffer at a flow rate of 2.0 mL/min. The purity of the preparations was ascertained by SDS−PAGE and staining with Bio-Safe Coomassie; the protein concentration was determined using the Bio-Rad dye-binding reagent with BSA as the standard. The yield from a 10 L culture was 18 mg.

NTPase Assays. The reaction mixtures (100 μL) contained 40 mM Tris-HCl, pH 7.5, 2 mM DTT, 20 μM poly(A) (Amersham) (given as the concentration of nucleotides), and Prp22 as indicated. The concentrations of NTPs and dNTPs, premixed with equimolar amounts of Mg^{2+}, were varied between 0.1 and 2 mM. In standard measurements, the ATP-Mg concentration was 2 mM, and the assay mixtures were incubated for 2 min at 23 °C. The reactions were quenched by addition of 1 mL of Biomol Green reagent (Biomol Research Laboratories, Plymouth Meeting, PA), and the absorbance at 620 nm was measured after 20 min at 23 °C. The amount of released phosphate was calculated by interpolation of the A_{620} values to a phosphate standard curve. Kinetic parameters were determined by nonlinear regression and Lineweaver−Burk plots using the EnzymeKinetics program (Trinity Software).

Double-Filter RNA-Binding Assay. The double-filter RNA-binding assay developed by Wong et al. (*21*) was adapted for measurements of Prp22−RNA binding. Nitrocellulose (8.5 × 13.5 cm, 0.2 μm) and nylon membranes (Hybond-N+) were purchased from Bio-Rad and Amersham, respectively. Nitrocellulose filters were presoaked in 0.5 M NaOH for 10 min and rinsed in H_2O until the pH was neutral. Nylon filters were washed once in 0.1 M EDTA (pH 8.8) and three times in 1.0 M NaCl for 10 min each, followed by rinsing with 0.5 M NaOH and washing with H_2O until the pH became neutral. Nitrocellulose and nylon filters were equilibrated in binding buffer (40 mM Tris-HCl, pH 7.4, 2 mM DTT, 1 mM EDTA, 10% glycerol) at 4 °C for at least 1 h prior to use. A 96-well dot-plot apparatus (Schleicher & Schuell) was assembled so that the nylon membrane was placed underneath the nitrocellulose filter.

Reaction mixtures (50 μL) containing 40 mM Tris-HCl, pH 7.5, 2 mM DTT, 2 mM $MgCl_2$, between 140 and 300 pM (3000−5000 cpm) ^{32}P-labeled nucleic acid, and varying amounts of Prp22 were incubated for 10 min at room temperature. Each well was washed with ice-cold binding buffer (200 μL) just prior to loading of the sample. Vacuum was applied, and the wells were washed twice with 100 μL of ice-cold binding buffer. The apparatus was disassembled, and the two filters were air-dried and then visualized and analyzed using a Phosphorimager and ImageQuant (Molecular Dynamics). The ratio of RNA that was bound to Prp22 was calculated using the following formula: $\text{bound RNA (\%)} = 100[(\text{signal}_{\text{nitrocellulose}})/(\text{signal}_{\text{nitrocellulose}} + \text{signal}_{\text{nylon}})]$. Each datum shown for the RNA-binding assays is the average of at least two measurements.

Preparation of Substrates for RNA Helicase Assay. The structures of the substrates used are summarized in Figure 6. The helicase substrates consisted of a longer unlabeled top strand and a ^{32}P-labeled bottom strand. A 99-mer RNA strand (5′-GGGCGAAUUGGGCCCUCUAGAUGCAUGCUCGAGCGGCCGCCAGUGUGAUGGAUAUCUGCAGAAUUCGCCCUUAAACCAUAAUCAUACCAGUUUUGGCAG-3′) was synthesized by runoff transcription in vitro using T7 RNA polymerase (Fermentas). A 99 nucleotide DNA strand of the same sequence (with T in lieu of U) was purchased from Qiagen. The 99 nt RNA and DNA top strands were purified by denaturing PAGE. RNA and DNA oligomers were purchased from Dharmacon and Qiagen, respectively, and 5′ end-labeled with [γ-^{32}P]ATP using T4 polynucleotide kinase (Fermentas). The sequences of the bottom strands for the substrates shown in Figure 6A−F are (A) ^{32}P-GAGCATGCATCTAGAGGGCCCAATTCGCCC (a 30 nt RNA strand contained U in lieu of T) for the 3′-tailed duplex, (B) ^{32}P-CTGCCAAAACTGGTATGATTATGGTTTAAG (30-mer to generate the 5′-tailed duplex), (C) ^{32}P-CUAGAGGGCCCAAUUCGCCC (20-mer RNA to gen-

erate the 3′-tailed duplex), (D) ^{32}P-CATCACACTGGCGGCCGCTC (20-mer DNA), (E) 5′-GCGGCCGCTCGAGCATGCATCTAGAGGGCCCAATTCGCCC (unlabeled 40-mer), ^{32}P-GGGCGAATTCTGCAGATATCCATCACACTG (30-mer), and (F) 5′-CGCTCGAGCATGCATCTAGAGGGCCCAATTCGCCC (unlabeled 35-mer), 5′-TGCAGATATCCATCACACTGGCGGC (unlabeled 25-mer), and ^{32}P-CTGGTATGATTATGGTTTAAGGGCGAATTC (30-mer). Substrates G and H (Figure 6) were 5′-GAGCAUGCAUCUAGAGGGCCCAAUUCGCCC-3′ (unlabeled top strand); the bottom strands were (G) ^{32}P-GGCCCTCTAGATGCATGCTC (20-mer DNA) and (H) ^{32}P-GGGCGAAUUGGGCCCUCUAGAUGCAUGCUC (30-mer RNA). The top strands were annealed with an equimolar amount of the bottom strand oligonucleotides, and the hybrids were then purified by native gel electrophoresis as described (*22*). Note that, for substrates E and F (Figure 6), annealing of unlabeled oligonucleotides was necessary to prevent the formation of structures that migrated aberrantly on nondenaturing gels.

The ΔG values for the duplex segments of each substrate were calculated using the values established by the nearest neighbor method for RNA−RNA, RNA−DNA, and DNA−DNA helices (*23*−*25*). Note that those measurements were performed using conditions (e.g., 1 M NaCl) that were different from those used for these studies, and the calculated ΔG values therefore only represent approximations to the real free energies of the helices.

RNA Helicase Assay. Reaction mixtures (20 μL) containing 40 mM Tris-HCl, pH 7.5, 2 mM ATP, 2 mM MgCl, 2 mM DTT, 1.25 nM helicase substrate, and 25 nM Prp22 were incubated for 1 h at 30 °C. Reactions were stopped by transferring to ice and adding 5 μL of loading buffer [100 mM Tris-HCl, pH 7.4, 5 mM EDTA, 0.5% SDS, 50% glycerol, 0.1% (w/v) bromophenol blue and xylene cyanol dyes, 0.1% NP-40]. Samples were analyzed by electrophoresis through an 8% polyacrylamide gel (30:0.8 acrylamide:bisacrylamide) containing 50 mM Tris−borate, 1 mM EDTA, and 0.1% SDS. The radiolabeled samples were quantified using PhosphorImager and ImageQuant (Molecular Dynamics), and each datum shown for the helicase assays is the average of at least two measurements.

RESULTS

Stimulation of ATP Hydrolysis by RNA. His_{10}-tagged Prp22 was purified from a soluble bacterial lysate by Ni-NTA affinity chromatography, ammonium sulfate precipitation, and gel filtration. ATP hydrolysis was dependent on Mg^{2+}, and in all experiments ATP was premixed with equimolar amounts of Mg^{2+} to prevent inhibitory effects of free Mg^{2+}, which were observed when the Mg^{2+} concentration exceeded that of ATP (not shown). To determine the affinity of Prp22 for the RNA cofactor, ATP hydrolysis (at 2 mM ATP-Mg) was measured as a function of increasing concentrations of poly(A) (Figure 1A). The reaction kinetics followed the Michaelis−Menten model, and we determined the K_m for the RNA cofactor to be 1.6 μM [expressed as the concentration of AMP, because the poly(A) preparation was heterogeneous in length]. The ATPase activity of Prp22, measured at 2 mM ATP-Mg, was optimal at pH 7.5 and the turnover was 460 min^{-1} in the presence of poly(A) and 56 min^{-1} without cofactor (Figure 1A). These values agree with previously reported measurements of RNA-stimulated ATPase activity (*15*−*20*).

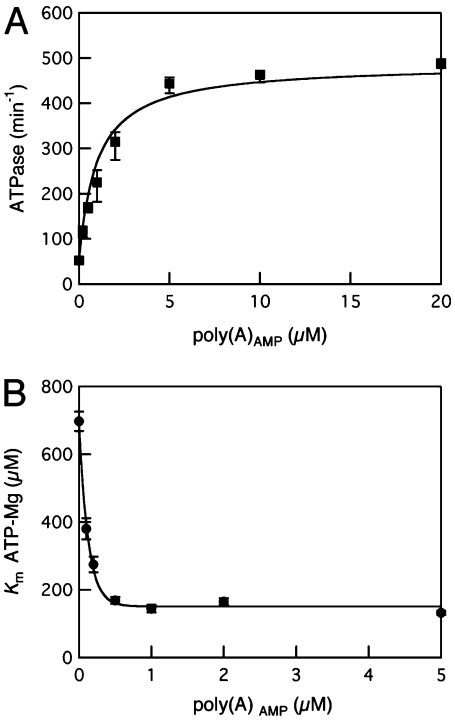

FIGURE 1: Influence of RNA on ATPase activity. (A) ATP hydrolysis (min^{-1}) was measured as a function of increasing concentrations of poly(A) RNA (expressed as concentration of nucleotide). The reaction mixtures contained 100 nM Prp22 and 2 mM ATP-Mg; the incubation time was 2 min. (B) The K_m values for ATP-Mg were determined at each indicated RNA concentration. The measurements were performed at six ATP-Mg concentrations between 0.1 and 2 mM. Each datum is the average from at least three measurements; the parameters were determined by Lineweaver−Burk plots using the EnzymeKinetics program (Trinity Software) and are plotted as a function of increasing concentrations of poly(A) in μM AMP.

The kinetic parameter K_m for ATP-Mg was determined at increasing poly(A) concentrations (Figure 1B). In the absence of RNA, the K_m was 700 μM. Increasing amounts of poly(A) led to a decrease of the K_m to 140 μM. The catalytic efficiency k_{cat}/K_m is increased 30-fold from 1.5×10^5 to 4.6×10^6 M^{-1} s^{-1} by poly(A). The increase in ATP hydrolysis by RNA is accompanied by a decrease in the K_m for the ATP substrate, suggesting that RNA binding elicits a conformational change in the ATP binding site of Prp22, so as to increase the protein's affinity for the substrate. A prior study reported that the K_m values for ATP were 95 and 103 μM in the presence and absence of RNA cofactor, respectively (*16*). Differences in the experimental conditions, e.g., the use of Mg^{2+} concentrations in excess of ATP in the prior study, might account for the discrepancy.

Effect of RNA Length on Stimulated ATP Hydrolysis. Stimulation of ATPase activity was assessed using a set of poly(A) oligomers of defined lengths (Figure 2A). The turnover number of Prp22 at 2 mM ATP-Mg was 56 min^{-1} in the absence of RNA. Inclusion of oligomers of 5, 10, 20, 30, and 40 nucleotides resulted in incrementally higher activities (96, 240, 270, 310, and 320 min^{-1}, respectively). The concentration of RNA at which the reaction velocity was half-maximal was 28, 29, 74, and 1080 nM for oligomers of 40, 30, 20, and 10 nt in length, respectively (Figure 2B).

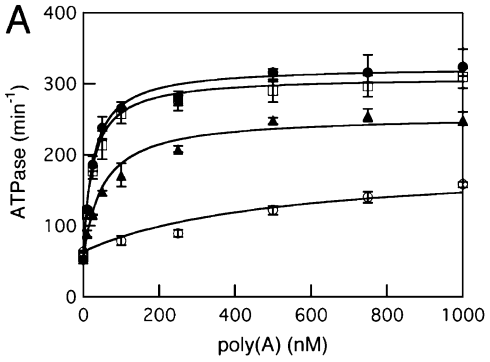

B

	ATPase (min^{-1})	$K_{m\ RNA}$ (nM)
$poly(A)_{40}$	320	28
$poly(A)_{30}$	310	29
$poly(A)_{20}$	270	74
$poly(A)_{10}$	240	1080
$poly(A)_5$	96	n.d.
–	56	–

FIGURE 2: Effect of RNA length. (A) ATPase activity (in min^{-1}) was measured as a function of increasing concentrations of poly(A) oligomers of 10 (○), 20 (▲), 30 (□), and 40 (●) nucleotides in length. The concentrations of Prp22 and ATP-Mg were 100 nM and 2 mM, respectively. (B) The kinetic parameters k_{cat} and $K_{m\ RNA}$ were determined by nonlinear regression. Measurements with $poly(A)_5$ and $poly(A)_{10}$ were performed at RNA concentrations up to 4 mM. RNA saturation could not be attained with $poly(A)_5$, and a $K_{m\ RNA}$ value could not be determined (n.d.).

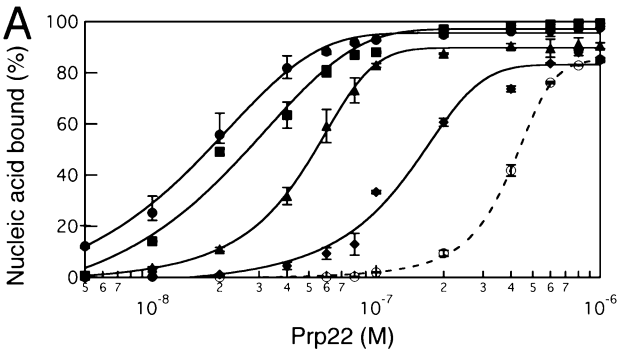

B

Nucleic Acid	apparent K_D (nM) – ATP	+ ATP
$poly(A)_{40}$	17	46
$poly(A)_{30}$	26	100
$poly(A)_{20}$	50	160
$poly(A)_{10}$	140	370
$poly(dA)_{40}$	400	–

FIGURE 3: Nucleic acid binding. (A) Increasing concentrations of Prp22 were incubated with ^{32}P-labeled nucleic acid in the absence of ATP and then filtered through nitrocellulose. The percentage of nucleic acid bound was plotted as a function of Prp22 concentration (logarithmic scale). The symbols are $poly(A)_{40}$ (●), $poly(A)_{30}$ (■), $poly(A)_{20}$ (▲), $poly(A)_{10}$ (◆), and $poly(dA)_{40}$ (○). (B) The apparent K_D values (in nM) reflect the concentration of Prp22 at which 50% of ^{32}P-labeled nucleic acid was bound. Incubations were performed in the absence (−ATP) or presence (+ATP) of 2 mM ATP-Mg.

The catalytic efficiency $k_{cat}/K_{m\ RNA}$ was 13- and 40-fold higher for a 20- and 30-mer, respectively, compared to that of a 10-mer. Stimulation of Prp22's ATPase activity was specific for single-stranded RNA, insofar as $poly(dA)_{40}$ had no effect on ATP hydrolysis (not shown).

In summary, there is a direct correlation between the length of the RNA cofactor and the stimulatory effect on the ATPase activity of Prp22, whereby long RNAs are more effective than shorter (<20 nt) RNAs.

Nucleic Acid Binding. Prior studies, using native PAGE, showed that Prp22 could form complexes with RNA (*19*, *26*). We now used a double-filter RNA-binding assay (*21*) to measure the relative affinity of Prp22 for nucleic acids. ^{32}P-Labeled nucleic acid (between 140 and 300 pM) was incubated with increasing amounts of Prp22 (5 nM to 1 μM), and the mixture was then filtered through a nitrocellulose membrane for retention of nucleic acid−protein complexes. Free nucleic acids were captured on a nylon membrane placed underneath the nitrocellulose. We express the relative binding affinity (K_D) as the concentration of Prp22 at which 50% of the nucleic acid was bound.

The affinity of Prp22 for a 40-mer oligonucleotide $poly(A)_{40}$ was 17 nM (Figure 3). The binding curve for $poly(A)_{30}$ was similar, with an apparent K_D of 26 nM. Incrementally higher Prp22 concentrations were necessary to achieve binding of $poly(A)_{20}$ and $poly(A)_{10}$, resulting in a shift of the binding curves to the right in Figure 3A. The K_D values were 50 and 140 nM for the 20- and 10-mer, respectively. The K_D for DNA, $poly(dA)_{40}$ was 400 nM, 20-fold higher than for the corresponding $poly(A)_{40}$ (Figure 3B). At concentrations of up to 10 μM, $poly(dA)_{40}$ had no stimulatory effect on the ATPase activity of Prp22, and a 100-fold excess of $poly(dA)_{40}$ over $poly(A)_{40}$ did not inhibit the RNA-stimulated ATPase activity of Prp22 (not shown). These findings suggest that the weak DNA binding is not through the RNA-binding site(s) of Prp22.

We investigated the relative affinities of Prp22 for RNAs other than poly(A) (Figure 4). The K_D for nonhomopolymeric single-stranded 30- and 20-mer RNAs was 36 and 44 nM, respectively, similar to the values for $poly(A)_{30}$ and $poly(A)_{20}$ (26 and 50 nM). For a RNA−RNA duplex that lacked a single-stranded tail (Figure 6H), the K_D value was 360 nM (Figure 4B). We conclude that Prp22 has a preference for binding to single-stranded RNA over single-stranded DNA or duplex nucleic acids and that the relative RNA-binding affinity increases with the length of the single-stranded RNA.

When we assessed binding of duplex nucleic acids used for unwinding assays, there was a correlation between the length of the single-stranded overhang and the relative binding affinity, insofar as higher concentrations of Prp22 were necessary to achieve half-maximal binding of substrates with short overhangs (Figure 4B). However, it appears that the polarity of the junction between the single- and double-stranded segments might also influence Prp22 binding, because the K_D values for the 5′- and 3′-tailed substrates (the single-stranded segment was 69 nt in both cases) were 62 and 14 nM, respectively.

Effect of ATP on RNA Binding. Inclusion of 2 mM ATP-Mg in RNA-binding assays resulted in a shift of the binding curves for each of the RNA oligomers tested. The apparent K_D values were increased from 17 to 46 nM for $poly(A)_{40}$, from 26 to 100 nM for $poly(A)_{30}$, from 50 to 160 nM for

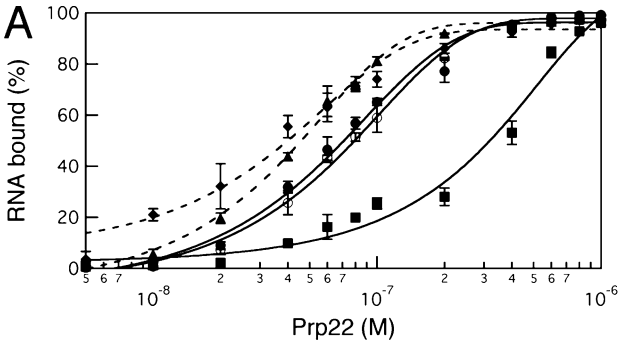

B

		single strand (nt)	apparent K_D (nM)
◆ 5′ 3′ *	RNA	30	36
▲ *	RNA	20	44
■ *—	RNA/RNA	0	360
● *—	RNA/RNA	10	68
○ *—	RNA/DNA	10	77
—*	RNA/DNA	69	14
—*	RNA/DNA	69	62
*—	RNA/RNA	79	10

FIGURE 4: Binding of Prp22 to various polymers. (A) The percentage of ^{32}P-labeled nucleic acid bound to nitrocellulose filters (%) is plotted as a function of Prp22 concentration (logarithmic scale). The symbols are 30-mer RNA (◆), 20-mer RNA (▲), 30 bp RNA−RNA duplex (■), 20 bp RNA−RNA duplex with a 10 nt 3′-tail (●), and 20 bp RNA−DNA duplex with a 10 nt 3′-tail (○). Dashed lines indicate single-stranded RNA; solid lines indicate duplex polymers. (B) Summary of the binding parameters (apparent K_D) for nucleic acid polymers. The structures and the length of the single-stranded segments (in nt) are indicated for each of the polymers.

poly(A)$_{20}$, and from 140 to 370 nM for poly(A)$_{10}$ (Figure 3B). We surmise that Prp22 dissociates from the RNA upon ATP hydrolysis, resulting in the observed reduction in apparent RNA-binding affinity. ATP hydrolysis, rather than binding, appeared to be required, insofar as the nonhydrolyzable ATP analogue AMP-PCP had no effect on RNA binding (not shown).

Mapping of the Nucleic Acid Binding Site. The 1145 amino acid Prp22 protein consists of two functional domains, an N-terminal component (1−480) that has no catalytic function per se and a C-terminal ATPase−helicase component (466−1145) that has ATPase and RNA unwinding activities (*26*). The two domains can function in pre-mRNA splicing in vivo when expressed as separate polypeptides (*26*). Here we tested the RNA-binding properties of two N-terminal deletion mutants, Prp22(262−1145) and Prp22(466−1145) (Figure 5). The K_D values of Prp22(262−1145) and Prp22(466−1145) for poly(A)$_{40}$ were 13 and 26 nM, respectively. In the presence of 2 mM ATP-Mg, the K_D increased to 53 nM for Prp22(262−1145) and to 90 nM for Prp22(466−1145) (Figure 5). These values were similar to full-length Prp22 (Figure 3B). We also tested the RNA-binding capacity of the N-terminal segment, Prp22(1−480). The K_D value for poly(A)$_{40}$ was 140 nM, 5−10-fold above the values for either native Prp22 or the C-terminal ATPase domains. RNA binding of the catalytically inert N-terminal domain was not affected significantly by inclusion of ATP-Mg in the reaction mix (Figure 5C). We conclude that the high-affinity RNA-binding site responsible for ATPase activation resides within the C-terminal domain.

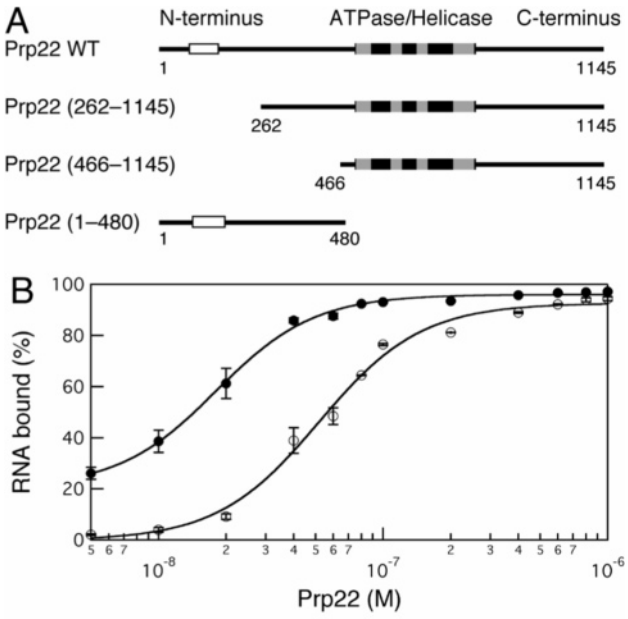

C

Protein	apparent K_D (nM) − ATP	+ ATP
Prp22 (262–1145)	13	53
Prp22 (466–1145)	26	90
Prp22 (1–480)	140	170

FIGURE 5: Effect of ATP on RNA binding. (A) Schematic depiction of the 1145 amino acid Prp22 protein and of truncated mutant proteins. The open box in the N-terminal portion indicates a peptide motif spanning residues 177−256, a so-called "S1 motif" that is found in many nucleic acid binding proteins including the ribosomal S1 protein from bacteria (*14*). The shaded boxes indicate peptide motifs that are important for ATP hydrolysis and helicase activity. (B) The percentage of poly(A)$_{40}$ retained on nitrocellulose is plotted as a function of increasing concentrations of Prp22(262−1145) (●). The open symbols (○) demarcate the binding curve that was obtained when 2 mM ATP-Mg was included in the reaction mixtures with Prp22(262−1145). (C) A summary of the relative binding affinities (apparent K_D values) measured in the presence and absence of 2 mM ATP-Mg.

Prp22 Is a Unidirectional 3′ to 5′ RNA Helicase. Prior studies showed that Prp22 could unwind 3′-tailed RNA substrates and 5′/3′-tailed RNA duplexes (*15*, *16*). To clarify the directionality and to determine the requirements for unwinding, we tested a series of RNA−DNA, RNA−RNA, and DNA−DNA substrates that differed with respect to the length of the duplex region and the polarity (3′ or 5′) and length of the single-stranded overhangs (Figure 6).

Prp22 unwound a 30 bp RNA−DNA duplex containing a 3′ single-stranded tail (Figures 6A and 7A). The product accumulated steadily over 30 min and plateaued with 75% unwound at 60−90 min (Figure 7B). A molar excess of enzyme over substrate (20:1) was required to attain optimal unwinding, indicating that few of the binding events were productive; i.e., Prp22 might bind and then dissociate upon ATP hydrolysis more often than it unwinds through the duplex segment. In contrast to the 3′-tailed duplex, Prp22 failed to unwind a 5′-tailed substrate over the course of 90 min (Figure 7B), even at protein concentrations of up to 200

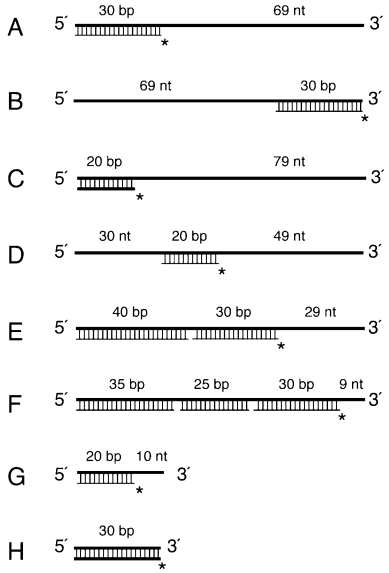

FIGURE 6: Schematics of helicase substrates. Thick lines indicate RNA strands, and thin lines represent DNA molecules. The asterisk (∗) marks the ^{32}P-labeled 5′ end of the annealed oligomer, and the number of base pairs (bp) and single-stranded segments (nt) is given in each case. (A) 3′-Tailed 30 bp RNA−DNA duplex. (B) 5′-Tailed 30 bp RNA−DNA duplex. (C) 3′-Tailed 20 bp RNA−RNA duplex. (D) 20 bp RNA−DNA duplex with 3′ and 5′ overhangs. (E) RNA−DNA duplex with a 29 nt 3′-tail. Two DNA oligomers were annealed, but only the 30-mer adjacent to the 3′-tail was ^{32}P-labeled. (F) RNA−DNA duplex with a 9 nt 3′-tail. Three DNA oligomers were annealed, but only the 30-mer adjacent to the 3′-tail was ^{32}P-labeled. (G) 20 bp RNA−DNA duplex with 10 nt 3′-tail. (H) 30 bp RNA−RNA duplex.

nM (not shown). We presume that the inability to unwind the 5′-tailed substrate was not caused by a difference in the duplex stability, insofar as the relative ΔG (kcal mol^{-1}) value was higher for the 5′-tailed duplex (−34.6) compared to the 3′-tailed substrate (−48.6) (Table 1). Furthermore, because no unwinding of the 5′-tailed duplex was observed at 200 nM Prp22, it appears unlikely that the substrate specificity could be fully accounted for by a difference in the apparent RNA-binding affinity as measured by filter binding in the absence of ATP (Figure 5). The finding that Prp22 could not unwind a 5′-tailed duplex demonstrates that Prp22 is a 3′ to 5′ helicase and that it requires a single-stranded segment. The 3′ overhang must be RNA, insofar as Prp22 did not catalyze unwinding of substrates with 3′ DNA overhangs, irrespective of whether the annealed strand was RNA or DNA (Table 1). This is consistent with the findings that Prp22 did not bind DNA with high affinity and that DNA did not stimulate ATP hydrolysis.

To assess the influence of duplex stability on unwinding, we varied the lengths of DNA oligonucleotides that were annealed to a 99 nt RNA. A 3′-tailed 30 bp RNA−DNA duplex (Figure 6A) was unwound efficiently by Prp22 (Figures 7 and 8); however, Prp22 unwound less than 5% of the substrate over 90 min when the annealed strand was a 30-mer RNA (Table 1). This was most likely caused by increased stability of the RNA−RNA helix compared to a RNA−DNA helix (−61.8 and −48.6 kcal mol^{-1}, respectively). When the 3′-tailed RNA−RNA duplex was shortened to 20 bp (−41.5 kcal mol^{-1}) (Figure 6C and Table 1), the rate and extent of unwinding were comparable to unwinding of the 3′-tailed 30 bp RNA−DNA duplex (Figure 8). A RNA−DNA duplex of 20 bp (−33.6 kcal mol^{-1}) that contained a 49 nt 3′-tail (Figure 6D) was efficiently unwound, and 85% of a 20 nt DNA oligomer was displaced by Prp22 within 20 min (Figure 8). These findings show that the relative stability of a nucleic acid duplex directly impacts on the unwinding activity of Prp22 and suggest that the processivity of Prp22 is poor.

Prp22 could efficiently unwind helices with 69 and 49 nt 3′ RNA overhangs (Figure 8 and Table 1). To determine the length requirement for the single-stranded segment, we annealed DNA oligonucleotides, so as to generate substrates with 29 and 9 nt 3′ overhangs (Figure 6E,F). A 30 nt oligomer adjacent to the 3′-tail was labeled and its displacement was monitored. (Note that additional DNA oligonucleotides were annealed to prevent formation of potential secondary structures within the single-stranded RNA.) Prp22 unwound the substrates containing a 3′-tail of 29 and 9 nt less well than duplexes with longer 3′ overhangs, and the

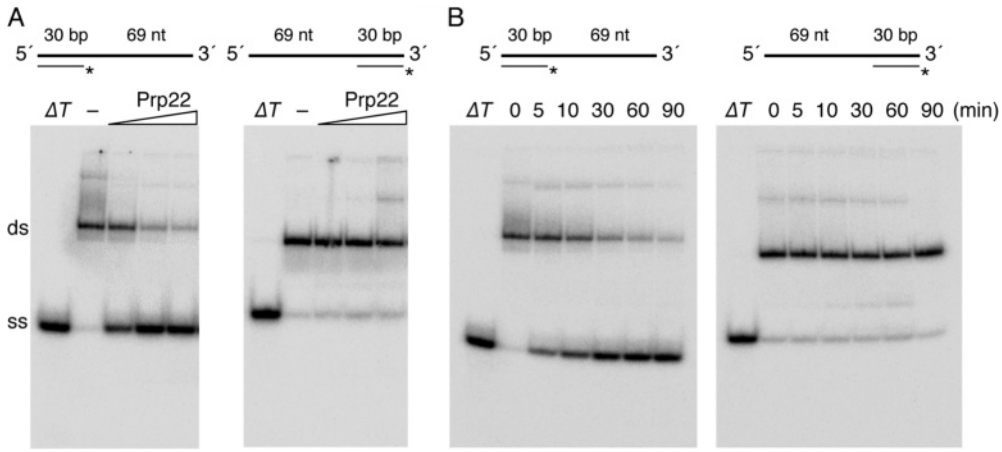

FIGURE 7: Directionality of duplex unwinding by Prp22. (A) Reaction mixtures containing 2 mM ATP and Mg^{2+}, 1.25 nM ^{32}P-labeled helicase substrates, depicted at the top, and increasing concentrations of Prp22 (10, 25, and 50 nM) were incubated for 1 h at 37 °C. The reaction mixtures were analyzed by native PAGE. ΔT shows migration of the labeled DNA oligonucleotide after heating of the substrate for 3 min at 95 °C, and (−) shows the substrate incubated in the absence of protein. (B) Reaction mixtures contained 25 nM Prp22 and 1.25 nM ^{32}P-labeled helicase substrates. Aliquots were withdrawn after the indicated times (min) and analyzed by native PAGE. ΔT shows migration of the labeled DNA oligonucleotide after heating of the substrate for 3 min at 95 °C. Autoradiograms of the dried gels are shown; the positions of the duplex (ds) and labeled single-strand (ss) nucleic acids are indicated at the left.

Table 1: Summary of Structures of Helicase Substrates and Calculated Free Energies (ΔG) of the Nucleic Acid Duplexes

structure	nucleotides	overhang (nt) 5′	overhang (nt) 3′	labeled duplex length (nt)	labeled duplex $\Delta G°_{37}$ (kcal/mol)[b]	unwinding[a]
5′ 3′	RNA/DNA	0	69	30	−48.6	+
	RNA/RNA	0	69	30	−61.8	−
	DNA/DNA	0	69	30	−43.2	−
	DNA/RNA	0	69	30	−47.4	−
	RNA/DNA	69	0	30	−34.6	−
	RNA/RNA	0	79	20	−41.5	+
	RNA/DNA	30	49	20	−33.6	+
	RNA/DNA	0	29	30	−41.4	+
	RNA/DNA	0	9	30	−36.5	+
	RNA/DNA	0	10	20	−32.2	+
	RNA/RNA	0	10	20	−40.9	+
	RNA/RNA	0	0	30	−61.8	−

[a] The ability of Prp22 to unwind each of the substrates is shown. (+) indicates that more than 5% of the duplex was unwound in 1 h under standard conditions; (−) indicates less than 5% unwinding. [b] The ΔG values for the duplex segments of each substrate were calculated using the values established by the nearest neighbor method for RNA−RNA, RNA−DNA, and DNA−DNA helices (*23*−*25*).

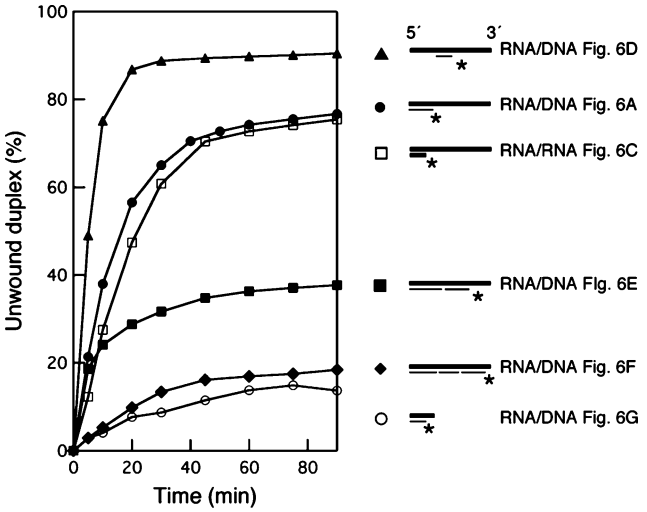

FIGURE 8: Unwinding of various substrates. Reaction mixtures contained 25 nM Prp22, 2 mM ATP-Mg, and 1.25 nM duplex substrates: a 20 bp RNA−DNA duplex with a 49 nt 3′ overhang (▲); a 30 bp RNA−DNA with a 69 nt 3′-tail (●); a 20 bp RNA−RNA duplex with a 79 nt 3′-tail (□); RNA−DNA duplex with a 29 nt 3′-tail (■); RNA−DNA duplex containing a 9 nt 3′-tail (◆); a 20 bp RNA−DNA duplex with a 10 nt 3′-tail (○). Aliquots were withdrawn after the indicated times and analyzed by native PAGE. The amount of unwinding (%) was quantified with the help of a Phosphorimager and was plotted as a function of time (min). The substrate structures are shown in the schematic drawings at the right; thick lines represent RNA, thin lines indicate DNA, and the asterisk marks the position of ^{32}P.

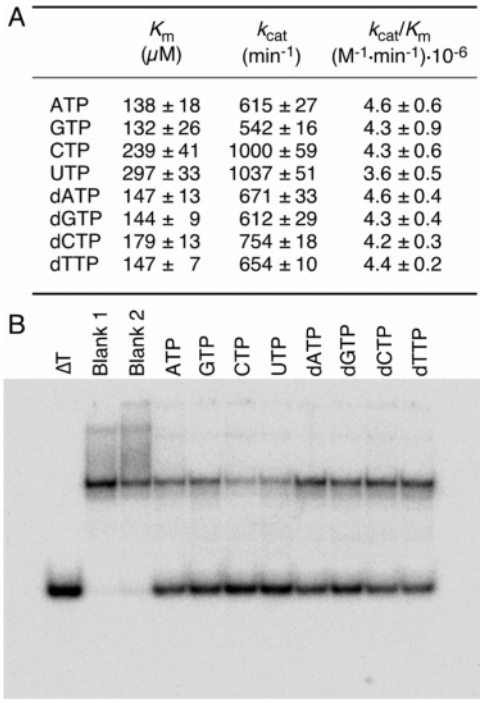

	K_m (μM)	k_{cat} (min^{-1})	k_{cat}/K_m (M^{-1}·min^{-1})·10^{-6}
ATP	138 ± 18	615 ± 27	4.6 ± 0.6
GTP	132 ± 26	542 ± 16	4.3 ± 0.9
CTP	239 ± 41	1000 ± 59	4.3 ± 0.6
UTP	297 ± 33	1037 ± 51	3.6 ± 0.5
dATP	147 ± 13	671 ± 33	4.6 ± 0.4
dGTP	144 ± 9	612 ± 29	4.3 ± 0.4
dCTP	179 ± 13	754 ± 18	4.2 ± 0.3
dTTP	147 ± 7	654 ± 10	4.4 ± 0.2

FIGURE 9: Prp22 uses all common NTPs and dNTPs. (A) Kinetic parameters for hydrolysis of nucleoside triphosphates were determined at 100 nM Prp22, various concentrations of a substrate and equimolar $MgCl_2$, 20 μM poly(A), and 2 mM DTT in 40 mM Tris-HCl (pH 7.5). The kinetic values are averages of at least six measurements. (B) 1.25 nM 3′-tailed 30 bp RNA−DNA duplex (Figure 6A) was incubated in the presence of NTP or dNTP (2 mM each, premixed with $MgCl_2$) as indicated. The control reaction lacked ATP and Prp22 (blank 1) or ATP only (blank 2). Reactions were analyzed by native PAGE, and an autoradiogram of the dried gel is shown. ΔT shows migration of the labeled DNA oligonucleotide after heating of the substrate for 3 min at 95 °C.

extent of unwinding was 35% and 15% in 90 min, respectively (Figure 8). The displacement of a 20 bp duplex carrying a 10 nt 3′-tail was similarly inefficient (Figures 6G and 8). We conclude that the length of the single-stranded RNA overhang is critical for efficient unwinding by Prp22 and that, when the tail length is 49 nt or longer, unwinding efficiency is primarily determined by the relative stability of the nucleic acid duplex.

Nucleoside Triphosphate Specificity. Prp22 was capable of hydrolyzing the nucleoside triphosphates ATP, GTP, CTP, and UTP and the deoxynucleoside triphosphates dATP, dGTP, dCTP, and dTTP (Figure 9). The k_{cat} values were between 542 min^{-1} for GTP and 1037 min^{-1} for UTP, and the K_m for the various substrates ranged from 132 μM for GTP to 297 μM for UTP (Figure 9A). The catalytic efficiencies (k_{cat}/K_m) were similar, showing that Prp22 did not exhibit significant specificity in NTP hydrolysis. Each of the NTPs and dNTPs supported unwinding of a duplex by Prp22 (Figure 9B).

DISCUSSION

The DEAH-box protein Prp22 plays an essential role in yeast mRNA splicing. Through ATP hydrolysis, Prp22

releases mRNA from the spliceosome. Prior in vitro analyses showed that ATPase activity is stimulated by RNA and that Prp22 is capable of unwinding duplex nucleic acids in an ATP-dependent fashion (*15*, *16*). Here we further characterized the helicase, NTPase, and RNA-binding activities of Prp22. The major findings are as follows: (i) Prp22 unwinds duplex nucleic acids containing single-stranded RNA tails with 3′ to 5′ directionality; (ii) Prp22 can hydrolyze all common ribo- and deoxyribonucleoside triphosphates; (iii) the RNA cofactor impacts on Prp22's ATPase activity by increasing k_{cat} and reducing the K_m for ATP; (iv) RNA-stimulated ATP hydrolysis, RNA-binding, and unwinding activities are affected concordantly by RNA chain length. It is instructive to compare the properties of Prp22 to those of other well-studied DExH-box proteins.

Prp22 hydrolyzes all common NTPs and dNTPs, a property that is shared by the related DEAH splicing factors Prp2 and Prp16 and also by the prototypical viral DExH helicases NPH-II from vaccinia virus and NS3 from hepatitis C (*27*−*31*). In contrast, other DExH proteins show a high degree of nucleotide substrate specificity. For example, the DNA helicase Rad3 hydrolyzes only ATP and dATP, whereas the human splicing factor U5-200kD can use ATP, dATP and CTP, dCTP but not GTP or UTP (*32*, *33*).

Prp22 binds to single-stranded RNA with high affinity but not to DNA or duplex nucleic acid. This preference is reflected in the ability of RNA versus DNA polymer to stimulate ATP hydrolysis. In contrast, NS3 and NPH-II can bind to RNA and DNA similarly, and their NTPase activity is stimulated by either RNA or DNA (*34*−*38*). The viral enzymes are selective for the length of the polynucleotide chain. NS3 exhibits optimal activity when the chain length is ≥12 nt (*35*), but it can bind to a 9-mer as visualized in a cocrystal structure (*39*). NPH-II prefers polynucleotides of ≥18 nt (*36*, *37*). Prp22 has a clear preference for RNAs that are 20−30 nt or longer. The length dependence may simply reflect a large physical binding site of Prp22; however, we cannot rule out the possibility that cooperative binding of multiple proteins to an RNA strand contributes to the effect.

Nucleic acid specificity for unwinding is generally determined by the chemical structure of the strand to which a directional helicase binds and translocates, the loading strand (*40*). Prp22 is an RNA helicase, whereas NS3 has the ability to unwind tailed RNA and DNA duplexes (*34*, *38*, *41*), mirroring the enzymes' polynucleotide specificities for binding and stimulated NTP hydrolysis. In contrast, RNA or DNA can stimulate the NTPase activity of NPH-II, yet NPH-II depends on RNA in the loading strand to efficiently unwind a tailed duplex (*36*, *42*).

DNA and RNA helicases are classified as 5′ → 3′, as 3′ → 5′, or as bidirectional, depending on the requirement for a 5′-tail, a 3′-tail, or either. It is now apparent that Prp22 unwinds duplexes with 3′ overhangs. The exemplary DExH helicases NPH-II and NS3 exhibit 3′ to 5′ directionality (*34*, *37*, *38*). In contrast, the DExH DNA helicase Rad3 has a strict 5′ to 3′ polarity (*32*). The splicing factor Prp16 prefers 3′-tailed substrates but can unwind duplexes with 5′ overhangs, albeit with reduced efficiency (*29*). We propose that Prp22, like other directional helicases, binds to the single-stranded segment and then, energized by NTP hydrolysis, moves along the RNA in the 3′ to 5′ direction and displaces annealed oligomers. However, unlike the RNA helicase NPH-II, which can unwind processively and displace multiple substrates per input enzyme (*36*, *43*), Prp22 can only displace duplexes of modest length and stability, and an excess of enzyme over substrate is required to accomplish unwinding. Thus, Prp22 is not a processive helicase. In the case of NS3, it was shown that the enzyme can unwind RNA but that it is a much more vigorous helicase on a DNA substrate; the processivity of NS3 on an RNA substrate is greatly increased by a cofactor, NS4A (*41*). Although it is conceivable that Prp22 requires a cofactor, or depends on a specific substrate to achieve processivity, it seems more likely that the enzymes' function in splicing does not necessitate unwinding of long helices.

Genetic suppression data suggested that Prp22 might act to disrupt contacts between the U5 snRNP and the spliced mRNA (ref *19* and unpublished data). Prp22 might accomplish this by unwinding a short U5 snRNA−mRNA helix or by destabilizing protein contacts that strengthen the inherently weak U5 snRNA−mRNA interaction (*44*, *45*). Prp22 clearly has the ability to disrupt RNA−RNA interactions. The alternative scenario in which Prp22 breaks stabilizing RNA−protein contacts is also plausible, because Prp22, like NPH-II, appears to be "blind" with respect to the displaced strand that can be either RNA or DNA. That RNA helicases can remodel RNP complexes and displace proteins from single-stranded RNAs has been demonstrated for NPH-II (*10*, *11*). The biochemical properties of Prp22 are compatible with the proposed model for how Prp22 releases mRNA, and the directionality has implications for the positioning of Prp22 on the RNA target.

REFERENCES

1. Burge, C. B., Tuschl, T. H., and Sharp, P. A. (1999) in *RNA World II* (Gesteland, R. F., Cech, T. R., and Atkins, J. F., Eds.) pp 525−560, Cold Spring Harbor Laboratory Press, Cold Spring Harbor, NY.
2. Madhani, H. D., and Guthrie, C. (1994) Dynamic RNA-RNA interactions in the spliceosome, *Annu. Rev. Genet. 28*, 1−26.
3. Staley, J. P., and Guthrie, C. (1998) Mechanical devices of the spliceosome: motors, clocks, springs, and things, *Cell 92*, 315−326.
4. Gorbalenya, A. E., and Koonin, E. V. (1993) Helicases: amino acid sequence comparisons and structure−function relationships, *Curr. Opin. Struct. Biol. 3*, 419−429.
5. Hall, M. C., and Matson, S. W. (1999) Helicase motifs: the engine that powers DNA unwinding, *Mol. Microbiol. 34*, 867−877.
6. Tanner, N. K., and Linder, P. (2001) DExD/H box RNA helicases: from generic motors to specific dissociation functions, *Mol. Cell 8*, 251−262.
7. Lorsch, J. R., and Herschlag, D. (1998) The DEAD box protein eIF4A. 2. A cycle of nucleotide and RNA-dependent conformational changes, *Biochemistry 37*, 2194−2206.
8. Schwer, B. (2001) A new twist on RNA helicases: DExH/D box proteins as RNPases, *Nat. Struct. Biol. 8*, 113−116.
9. Von Hippel, P. H. (2004) Helicases become mechanistically simpler and functionally more complex, *Nat. Struct. Mol. Biol. 11*, 494−496.
10. Jankowsky, E., Gross, C. H., Shuman, S., and Pyle, A. M. (2001) Active disruption of an RNA-protein interaction by a DExH/D RNA helicase, *Science 291*, 121−125.
11. Fairman, M. E., Maroney, P. A., Wang, W., Bowers, H. A., Gollnick, P., Nilsen, T. W., and Jankowsky, E. (2004) Protein displacement by DExH/D "RNA helicases" without duplex unwinding, *Science 30*, 730−734.
12. Kistler, A. L., and Guthrie, C. (2001) Deletion of MUD2, the yeast homologue of U2AF65, can bypass the requirement for Sub2, an essential spliceosomal ATPase, *Genes Dev. 15*, 42−49.

13. Chen, J. Y.-F., Stands, L., Staley, J. P., Jackups R. R., Jr., Latus, L. J., and Chang T.-H. (2001) Specific alterations of U1-C protein or U1 small nuclear RNA can eliminate the requirement of Prp28, an essential DEAD box splicing factor, *Mol. Cell 7*, 227−232.
14. Company, M., Arenas, J., and Abelson, J. (1991) Requirement of the RNA helicase-like protein PRP22 for release of messenger RNA from spliceosomes, *Nature 349*, 487−493.
15. Schwer, B., and Gross, C. H. (1998) Prp22, an RNA-dependent ATPase, plays two distinct roles in yeast pre-mRNA splicing, *EMBO J. 17*, 2086−2094.
16. Wagner, J. D. O., Jankowsky, E., Company, M., Pyle, A. M., and Abelson, J. N. (1998) The DEAH-box PRP22 is an ATPase that mediates ATP-dependent release from spliceosomes and unwinds RNA duplexes, *EMBO J. 17*, 2926−2937.
17. Schwer, B., and Meszaros, T. (2000) RNA helicase dynamics in pre-mRNA splicing, *EMBO J. 19*, 6582−6591.
18. Schneider, S., Hotz, H. R., and Schwer, B. (2002) Characterization of dominant-negative mutants of the DEAH-box splicing factors Prp22 and Prp16, *J. Biol. Chem. 277*, 15452−15458.
19. Schneider, S., Campodonico, E., and Schwer, B. (2004) Motifs IV and V in the DEAH box splicing factor Prp22 are important for RNA unwinding, and helicase-defective Prp22 mutants are suppressed by Prp8, *J. Biol. Chem. 279*, 8617−8626.
20. Campodonico, E., and Schwer, B. (2002) ATP-dependent remodeling of the spliceosome: Intragenic suppressors of release-defective mutants of *Saccharomyces cerevisiae* Prp22, *Genetics 160*, 407−415.
21. Wong, I., and Lohman, T. M. (1993) A double-filter method for nitrocellulose-filter binding: application to protein-nucleic acid interactions, *Proc. Natl. Acad. Sci. U.S.A. 90*, 5428−5432.
22. Lee, C. G., and Hurwitz, J. (1992) A new RNA helicase isolated from HeLa cells that catalytically translocates in the 3′ to 5′ direction, *J. Biol. Chem. 267*, 4398−4407.
23. Freier, S. M., Kierzek, R., Jaeger, J. A., Sugimoto, N., Caruthers, M. H., Neilson, T., and Turner, D. H. (1986) Improved free-energy parameters for predictions of RNA duplex stability, *Proc. Natl. Acad. Sci. U.S.A. 83*, 9373−9377.
24. Sugimoto, N., Nakano, S., Katoh, M., Matsumura, A., Nakamuta, H., Ohmichi, T., Yoneyama, M., and Sasaki, M. (1995) Thermodynamic parameters to predict stability of RNA/DNA hybrid duplexes, *Biochemistry 34*, 11211−11216.
25. Sugimoto, N., Nakano, S., Yoneyama, M., and Honda, K. (1996) Improved thermodynamic parameters and helix initiation factor to predict stability of DNA duplexes, *Nucleic Acids Res. 24*, 4501−4505.
26. Schneider, S., and Schwer, B. (2001) Functional domains of the yeast splicing factor Prp22p, *J. Biol. Chem. 276*, 21184−21191.
27. Kim, S. H., Smith, J., Claude, A., and Lin, R. J. (1992) The purified yeast pre-mRNA splicing factor PRP2 is an RNA-dependent NTPase, *EMBO J. 11*, 2319−2326.
28. Schwer, B., and Guthrie, C. (1992) A conformational rearrangement in the spliceosome is dependent on PRP16 and ATP hydrolysis, *EMBO J. 11*, 5033−5039.
29. Wang, Y., Wagner, J. D., and Guthrie, C. (1998) The DEAH-box splicing factor Prp16 unwinds RNA duplexes in vitro, *Curr. Biol. 8*, 441−451.
30. Shuman, S. (1992) Vaccinia virus RNA helicase: an essential enzyme related to the DE-H family of RNA-dependent NTPases, *Proc. Natl. Acad. Sci. U.S.A. 89*, 10935−10939.
31. Wardell, A. D., Errington, W., Ciaramella, G., Merson, J., and McGarvey, M. J. (1999) Characterization and mutational analysis of the helicase and NTPase activities of hepatitis C virus full-length NS3 protein, *J. Gen. Virol. 80*, 701−709.
32. Naegeli, H., Bardwell, L., Harosh, I., and Friedberg, E. C. (1992) Substrate specificity of the Rad3 ATPase/DNA helicase of *Saccharomyces cerevisiae* and binding of Rad3 protein to nucleic acids, *J. Biol. Chem. 267*, 7839−7844.
33. Laggerbauer, B., Achsel, T., and Lührmann, R. (1998) The human U5-200kD DEXH-box protein unwinds U4/U6 RNA duplices in vitro, *Proc. Natl. Acad. Sci. U.S.A. 95*, 4188−4192.
34. Gwack, Y., Kim, D. W., Han, J. H., and Choe, J. (1996) Characterization of RNA binding activity and RNA helicase activity of the hepatitis C virus NS3 protein, *Biochem. Biophys. Res. Commun. 225*, 654−659.
35. Preugshat, F., Averett, D. R., Clarke, B. E., and Porter, D. J. T. (1996) A steady-state and pre-steady-state kinetic analysis of the NTPase activity associated with the hepatitis C virus NS3 helicase domain, *J. Biol. Chem. 271*, 24449−24457.
36. Gross, C. H., and Shuman, S. (1996) Vaccinia virus RNA helicase: nucleic acid specificity in duplex unwinding, *J. Virol. 70*, 2615−2619.
37. Shuman, S. (1993) Vaccinia virus RNA helicase: Directionality and substrate specificity, *J. Biol. Chem. 268*, 11798−11802.
38. Tai, C. L., Chi, W. K., Chen, D. S., and Hwang, L. H. (1996) The helicase activity associated with hepatitis C virus nonstructural protein 3 (NS3), *J. Virol. 70*, 8477−8484.
39. Kim, J. L., Morgenstern, K. A., Griffith, J. P., Dwyer, M. D., Thomson, J. A., Murcko, M. A., Lin, C., and Caron, P. R. (1998) Hepatitis C virus NS3 RNA helicase domain with a bound oligonucleotide: the crystal structure provides insights into the mode of unwinding, *Structure 6*, 89−100.
40. Lohman, T. M., and Bjornson, K. P. (1996) Mechanisms of helicase-catalyzed DNA unwinding, *Annu. Rev. Biochem. 65*, 169−214.
41. Pang, P. S., Jankowsky, E., Planet, P. J., and Pyle, A. M. (2002) The hepatitis C viral NS3 protein is a processive DNA helicase with cofactor enhanced RNA unwinding, *EMBO J. 21*, 1168−1176.
42. Kawaoka, J., and Pyle, A. M. (2005) Choosing between DNA and RNA: the polymer specificity of RNA helicase NPH-II, *Nucleic Acids Res. 33*, 644−649.
43. Jankowsky, E., Gross, C. H., Shuman, S., and Pyle, A. M. (2000) The DExH protein NPH-II is a processive and directional motor for unwinding RNA, *Nature 403*, 447−451.
44. Newman, A. J. (1997) The role of U5 snRNP in pre-mRNA splicing, *EMBO J. 16*, 5797−5800.
45. Teigelkamp, S., Newman, A. J., and Beggs, J. D. (1995) Extensive interactions of PRP8 protein with the 5′ and 3′ splice sites during splicing suggest a role in stabilization of exon alignment by U5 snRNA, *EMBO J. 14*, 2602−2612.

BI050407M